

Mechanical and electromagnetic properties of 3D printed hot pressed nanocarbon/poly(lactic) acid thin films

R. Kotsilkova, E. Ivanov, P. Todorov, I. Petrova, N. Volynets, A. Paddubskaya, P. Kuzhir, V. Uglov, I. Biró, K. Kertész, G. I. Márk, and L. P. Biró

Citation: *Journal of Applied Physics* **121**, 064105 (2017); doi: 10.1063/1.4975820

View online: <http://dx.doi.org/10.1063/1.4975820>

View Table of Contents: <http://aip.scitation.org/toc/jap/121/6>

Published by the [American Institute of Physics](#)

Articles you may be interested in

[Spin-dependent thermoelectric effects in graphene-based superconductor junctions](#)

Journal of Applied Physics **121**, 063903063903 (2017); 10.1063/1.4976005

[Field induced phase transitions and energy harvesting performance of \(Pb,La\)\(Zr,Sn,Ti\)O₃ single crystal](#)


Journal of Applied Physics **121**, 064104064104 (2017); 10.1063/1.4975786

[Tuning of acoustic wave dispersion in ferroelectrics—A theoretical study](#)

Journal of Applied Physics **121**, 064102064102 (2017); 10.1063/1.4975787

[Using gapped topological surface states of Bi₂Se₃ films in a field effect transistor](#)

Journal of Applied Physics **121**, 064301064301 (2017); 10.1063/1.4975819



Small Conferences. BIG Ideas.

Applied Physics
Reviews

SAVE THE DATE!
3D Bioprinting: Physical and Chemical Processes
May 2–3, 2017 • Winston Salem, NC, USA

Mechanical and electromagnetic properties of 3D printed hot pressed nanocarbon/poly(lactic) acid thin films

R. Kotsilkova,¹ E. Ivanov,^{1,2} P. Todorov,^{1,2} I. Petrova,¹ N. Volynets,³ A. Paddubskaya,^{3,4} P. Kuzhir,^{3,5} V. Uglov,⁶ I. Biró,⁷ K. Kertész,⁸ G. I. Márk,⁸ and L. P. Biró⁸

¹Open Laboratory on Experimental Micro and Nano Mechanics, Institute of Mechanics, Bulgarian Academy of Sciences, Acad. G. Bonchev Str., Block 4, Sofia, Bulgaria

²Research and Development of Nanomaterials and Nanotechnologies (NanoTech Lab Ltd.) Acad. G. Bonchev Str. Block 1, 1113 Sofia, Bulgaria

³Research Institute for Nuclear Problems, Belarusian State University, Bobruiskaya Str. 11, 220030 Minsk, Belarus

⁴Center for Physical Sciences and Technology, A. Goštauto 11, LT-01108 Vilnius, Lithuania

⁵Tomsk State University, Tomsk 634050, Russian Federation

⁶Belarusian State University, Nezavisimosti Sq. 2, Minsk 220030, Belarus

⁷3D Wishes, Bíró u. 44/a/2, Érd, Hungary

⁸Institute of Technical Physics and Materials Science, Centre for Energy Research, 1525 Budapest, P.O. Box 49, Hungary

(Received 2 December 2016; accepted 27 January 2017; published online 10 February 2017)

We constructed a new type of light-weight, nanocarbon based thin film material having good mechanical properties, thermal stability, and electromagnetic shielding efficiency. Our method, 3D printing combined with hot pressing, is a cheap and industrially upscalable process. First a sandwich structure was created by layer-to-layer deposition of alternating 100 μm thick nanocarbon containing plastic layers and 100 μm thick pristine plastic layers, repeated as building blocks. The 3D printed samples were hot pressed to obtain thin films of 10–30 μm thickness. We used a commercial nanocarbon 3D printing filament (Black Magic). TEM investigations revealed the nanocarbon filler to be a mixture of graphene sheets, short carbon nanotubes, fishbone nanotubes, graphitic nanoparticles, and carbon black. Small-angle X-ray scattering and X-ray diffraction studies showed some amorphization of the nanocarbon filler as a consequence of the hot pressing. The nanoindentation hardness, nanoscratch hardness, and Young's modulus increase gradually by increasing the number of layers in the films, due to an increase of the amount of nanocarbon filler. Microwave absorption also increases continuously with the number of nanocarbon layers, reaching 40% for 3 nanocarbon layers. We demonstrate that unlike most conventional composites loaded with nanocarbons having pronounced dielectric properties, when the real part of permittivity $Re(\epsilon)$ is much higher than its imaginary part $Im(\epsilon)$ at high frequencies, a combination of 3D printing and hot pressing allows the fabrication of composites with $Re \epsilon \approx Im \epsilon$ in a very broad frequency range (0.2–0.6 THz). Our new 3D printed—hot pressed thin films may compete with the CVD graphene sandwiches in electromagnetic shielding applications because of their easier processability and low cost. *Published by AIP Publishing.* [<http://dx.doi.org/10.1063/1.4975820>]

I. INTRODUCTION

The run-up of communication systems is responsible for a concomitant increase of the density of radio frequency emitters in the environment. As a result, the protection of sensitive electronic devices against external electromagnetic perturbations becomes a more and more stringent issue. Polymer films incorporating graphene and other nanocarbon fillers were recently studied as a light coating material to protect micro- and nano-devices in a harsh electromagnetic environment, due to the promising electromagnetic shielding efficiency of the carbon nanostructures.^{1,2}

Graphene has been demonstrated to be an interesting material in this context. For frequencies up to 100 GHz, the sheet conductivity of graphene produced by conventional CVD is a sizable fraction of the intrinsic admittance of air. Thanks to this nice coincidence, stacking a few layers of

graphene suffices to match the sum of the admittances of the media located on both sides, providing thereby the largest possible power absorption of electromagnetic radiations traveling from one medium to the other.^{3–5} However, it was found in our previous study that very thin CVD prepared graphene/polymer films are fragile and not easy to be produced and characterized due to the difficult sample handling.⁶ Therefore, stronger films and more reliable processing conditions are required to meet the different application needs, like, for example, nanocarbon based polymer composites.⁷ Many specific factors, e.g., thickness, microstructure and texture, and the degree of dispersion of fillers may have a strong influence on both the mechanical and the electromagnetic properties of nanocomposite films. Therefore, the design of reliable and functional thin films relies on the knowledge and understanding of their mechanical behavior when subjected to mechanical loading.⁸

Thin films with submicrometer thickness warrant load and displacement sensitivity in the sub-mN and sub- μm scales, hence their mechanical behavior has been rarely investigated.^{8,9} Recently, nano-indentation systems, which work in pico- to nano-Newton loading range and sub-micron displacement range, are found suitable for local characterization of thin films.^{10–14} The analysis of experiments and calculations of mechanical characteristics usually relies on the Oliver-Pharr method.^{11,12} For thin films however, the models cannot account for the elastic mismatch between film and substrate, depending on whether the film is softer or harder than the substrate. When the indentation depth becomes of the order of magnitude of the film thickness, there are some indications that the above mentioned indentation models can provide erroneous values of the Young's modulus of the layers.^{13,14}

In the present study, we propose an additive manufacturing combined with hot pressing, as a straightforward and industrially upscalable method to produce nanocarbon doped thin polymer films having good mechanical properties and at the same time, good electromagnetic shielding efficiency. It is also important to explore what a procedure like hot pressing does to the nanocarbon based composite.

Surface mechanical properties of the thin films at micro and nanoscale and their electromagnetic characteristics were determined depending on the initial number of nanocarbon layers. The applicability of the nanocarbon containing thin films as lightweight coatings for the protection of micro and nano-electronic devices, to low power microwave signals is discussed.

II. EXPERIMENTAL

A. Materials

The source material for 3D printing was a commercial composite filament Black Magic¹⁵ based on polylactic acid (PLA) thermoplastic doped with highly conductive nanocarbon filler(s). Undoped PLA based commercial filament was also used. The multilayered structure of the starting 3D printed samples was fabricated by layer-to layer deposition of alternating 100 μm PLA layer and 100 μm Black Magic layer (BML), repeated as building blocks. Thus, multilayered samples containing a 300 μm thick base PLA layer followed by one to three building blocks were produced by using Fused Filament Fabrication/Fused Deposition Modeling (FFF/FDM) 3D printer with dual head extruder (Extruder temperature: 230 °C; table heating: 50 °C; speed: 30 mm/s; extrusion multiplier). The 3D printed disk samples were hot pressed for 6 min, at 190 °C, applying a 100 Bar pressure to obtain thin films of thickness ~ 10 –30 μm . Thin films containing 1 to 3 Black Magic layers were produced, named here: BML1, BML2, and BML3. Reference samples consisting of undoped PLA layers were also produced for comparison.

B. Scanning electron microscope (SEM) and TEM analysis

Transmission Electron Microscope (TEM) at an accelerating voltage 200 kV was used for analysis of the residue

chart after burning of the polymeric film. For this study, a preliminary preparation technique was applied. A micro-quantity of water based char suspension was dropped on standard copper TEM grid covered by membrane from amorphous carbon and was dried after that in dust-free atmosphere at ambient conditions, and then visualized at different magnifications.

Scanning Electron Microscope (SEM) Philips 515 at accelerating voltage 25 kV and 5 kV was performed to study the morphology of the film's cross section. Before the examination in the microscope, the samples were cut in the liquid nitrogen, and the cross section was covered with a metal layer for better conductivity of the surface and to avoid charging effects.

C. Small-angle X-ray scattering (SAXS) and XRD analysis

X-ray diffraction (XRD) analysis was employed for structural identification using an Ultima IV X-ray diffractometer operating in parallel beam configuration and equipped with a CuK α wavelength (0.154179 nm) and a *scintillation* detector. SAXS spectra were obtained using the same geometry and 0.3 incidence angle.

D. Nanoindentation test

The nanoindentation test was performed, using the Universal Nanomechanical Tester (Bruker[®], USA). Rectangular samples of 10 \times 10 mm lateral size were cut from the pressed films and placed on a polycarbonate substrate. The tip used for the nanoindentation process was a Berkovich Diamond with a tip radius of 70 nm. The test was performed at a force of 30 mN and a temperature of 20 °C, consisting of 48 indentations made at different locations on the sample surface. Every single indentation experiment consists of the following subsequent steps: (i) approaching the surface; (ii) loading to the peak load of 30 mN for 15 s; (iii) holding the indenter at a peak load for 10 s; (iv) unloading from maximum force to 10% for 15 s; (v) holding at 10% of max. force for 15 s; (vi) final complete unloading for 1 s (load function 15–10–15 s trapezoid). The first hold step (iii) was included to avoid the influence of the creep on the unloading characteristics of a viscoelastic material since the unloading curve was used to obtain the elastic modulus of the material.¹⁶ To properly determine the initial contact point and the accurate contact area, the pull-in interaction was accounted for in our nanoindentation experiments, as pointed by Wang *et al.*¹⁷ The Oliver-Pharr model was used for the calculation of hardness (H) and Young's modulus of elasticity (E)^{11,12}

$$H = \frac{P}{A}, \quad (1)$$

$$\frac{1}{E_r} = \frac{1 - \nu^2}{E} + \frac{1 - \nu_i^2}{E_i}, \quad (2)$$

where P is the indenter load, A the projected contact area at that load, ν is the Poisson's ratio of the test material, E_i the

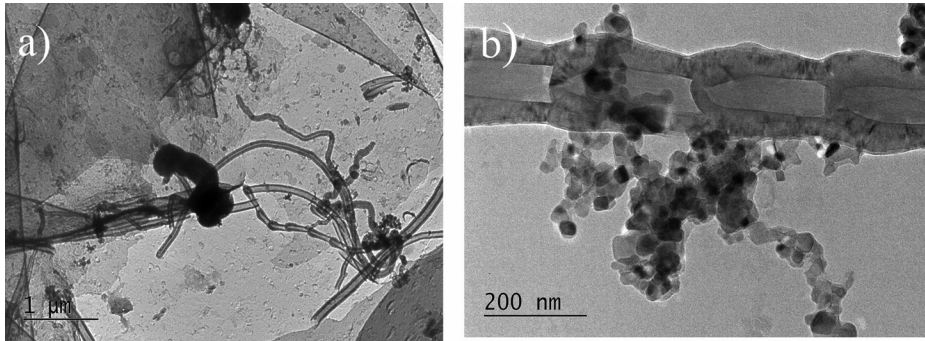


FIG. 1. ((a) and (b)) TEM micrographs of the residue carbon ash obtained after burning of the polymer in the hot pressed film at 500 °C.

modulus of the indenter, ν_i —the Poisson's ratio of the indenter, and E_r is the reduced modulus.

For a diamond-tipped indenter, $E_i = 1141$ GPa and $\nu_i = 0.07$ GPa, thus the second term of the equation becomes negligible. The aforementioned procedure was used to calculate the hardness and modulus at the maximum penetration depth from a single load–unload indent cycle.

E. Nanoscratch test

The Universal Mechanical Tribometer UMT-2M0 (Bruker®, USA) was used for carrying out the nanoscratch experiments. A diamond conical indenter with a spherical tip having a 2.5 μm radius was mounted on a 500 mN force sensor and was used to produce 10 scratches (in the same direction) on the surface of each of the films. The following scratch parameters were determined—scratch coefficient of friction (SCOF), μ_s ; corresponding normal force, F_Z (mN); and scratch hardness, H_S (GPa)—at a maximum penetration depth of 10 μm and scratch length of 5 mm. The friction force F_f was also determined for the sake of completeness.

The scratch hardness, H_S was calculated using the following equation:¹⁸

$$H_S = \frac{8F_z}{\pi b^2}, \quad (3)$$

where F_Z is the applied normal load and b is the scratch track width, observed via an optical microscope. The scratch coefficient of friction (SCOF), μ_s represents the ratio between the tangential and the normal load, $\mu_s = F_x/F_Z$. The friction force is also equal to the normal force F_Z multiplied by the coefficient of friction, $F_f = \mu_s F_Z$

F. Electromagnetic characterization

The microwave measurements in frequency range from 26 GHz to 37 GHz were provided by a Scalar Network Analyzer R2-408R, ELMIKA, Lithuania, at room temperature. The transmitted/input (S_{21}) and reflected/input (S_{11}) signals have been measured with a frequency stability 10^{-6} and power stability $7.0 \text{ mW} \pm 10 \mu\text{W}$. Measurement errors of S_{21} were $\delta|S_{21}| = \pm (0.6 + 0.06|S_{21}|)$. Reflectance (R), transmittance (T), and absorbance (A) were obtained from measured S-parameters as $R = S_{11}^2$, $T = S_{21}^2$, $A = 1 - R - T$. THz time-domain spectrometer, T-SPEC Ekspla, Lithuania, was used for THz experiments (see Ref. 7 for measurement details). Spectrometer is based on the femtosecond laser (wavelength 1 μm , pulse duration less than 150 fs) and GaBiAs photoconductive switch as THz emitter and detector working at 100 GHz–3 THz.

III. RESULTS AND DISCUSSION

A. Microstructure and morphology

The nanocarbon filler inside the hot pressed films was characterized by heating from 30 to 500 °C at a heating rate of 10 °C/min. At these heating conditions, the polymer in the film is fully burned, and the residue char contains only the nanocarbon filler, which remains non-degraded at these temperatures. Figs. 1(a) and 1(b) present the TEM micrographs of the carbon ash residue obtained after burning the polymer in the film. As seen, the nanocarbon filler is a complex mixture of graphene sheets, short carbon nanotubes including fishbone carbon nanotubes, graphitic nanoparticles, and carbon black.

In Fig. 2(a), an optical image of the cross section of the starting 3D printed specimen was presented. The multilayered structure of alternating PLA (transparent) layer and the Black Magic layer (BML), repeated four times is visualized,

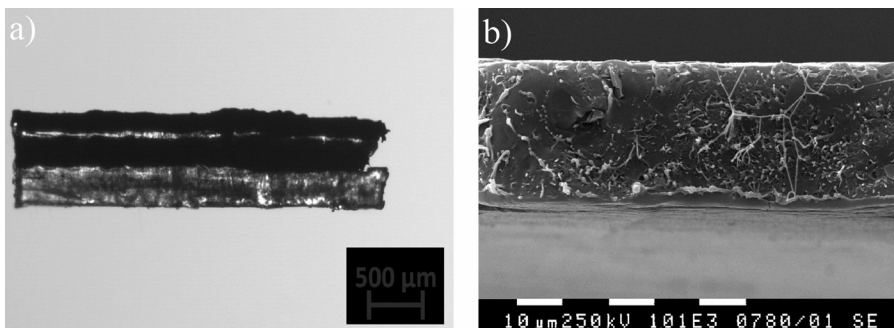


FIG. 2. ((a) and (b)) Cross section of: (a) the starting 3D printed multilayered specimen (optical image), and (b) the thin film after hot pressing of the starting specimen (SEM micrograph).

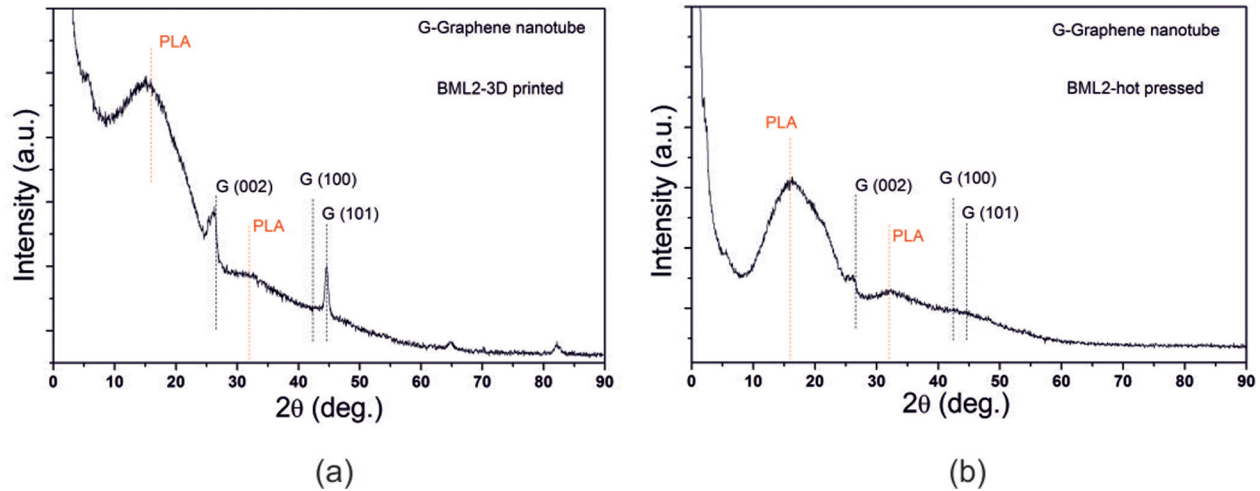


FIG. 3. SAXS spectra of: (a) starting 3D printed sample BML2-3D printed, and (b) BML2-hot pressed film.

and the thickness of the initial sample is measured of $\sim 1000 \mu\text{m}$. Fig. 2(b) shows a SEM micrograph of the cross section of the thin film, prepared by hot pressing of the 3D printed multilayered sample containing 3 BML layers. During hot pressing, the 3D printed sandwich structure almost disappeared as the BML layer is infiltrated into the PLA layer forming a homogeneously colored structure. Black Magic filament has a given, fixed concentration of nanocarbon. By this printing and pressing procedure, we can modify, alter the nanocarbon concentration and thus study indirectly the effect of this concentration on the properties.

B. SAXS and XRD characterization of the hot pressed films

Small angle X-ray analysis (SAXS) and standard X-ray analysis (XRD) were used to characterize the structure and the state of dispersion of nanocarbons in both the starting 3D printed multilayered samples and the hot pressed thin films. Both samples have the same composition, but differ in the post processing (hot pressing) applied to produce the film.

In Fig. 3 SAXS spectra of the starting 3D printed samples and the spectra of hot pressed films in both cases consisting of two carbon containing layers are presented. As PLA is a crystallizing polymer, then the formation of supramolecular structure is affected by its sample preparation technology, i.e., the cooling rate of the melt, the melt orientation. In Figure 3(a), there is a partial scattering of the X-ray beam at $2\Theta = 16^\circ$, which indicates a relatively small and defective crystals due to the rapid cooling of the melt during the printing process. At the same time, for hot pressed samples, a greater absorption was observed due to the slow cooling of the melt during the pressing process. The values of angles $2\Theta = 26.4^\circ$; 44.6° correspond to the hexagonal unit cell of crystallographic carbon structure. The G(002) and G(101) peaks almost disappear in the case of the hot pressed samples, which indicates some amorphization of the nanocarbon fillers. During the hot pressing process, the modification of the carbon structure such as a lateral shift of the layers (because the graphitic layers can easily be detached from each other) may take place under the influence of the applied load, which changes the inter-plane distance in

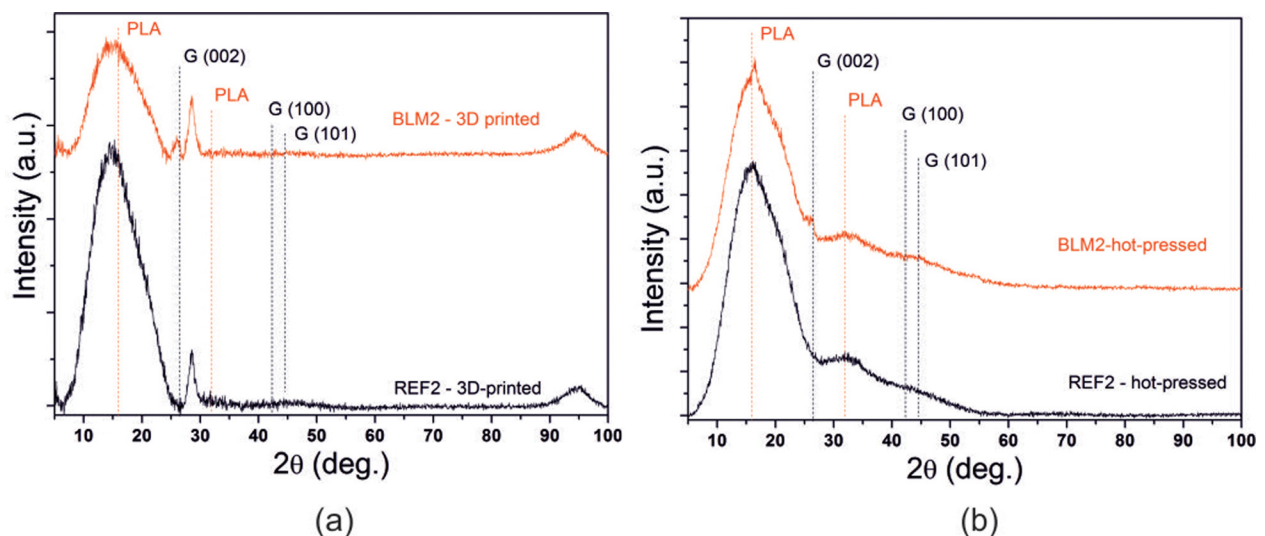


FIG. 4. XRD spectra of: (a) 3D printed starting sample, and (b) hot pressed film; G002 peak appears in Fig. 4(a).

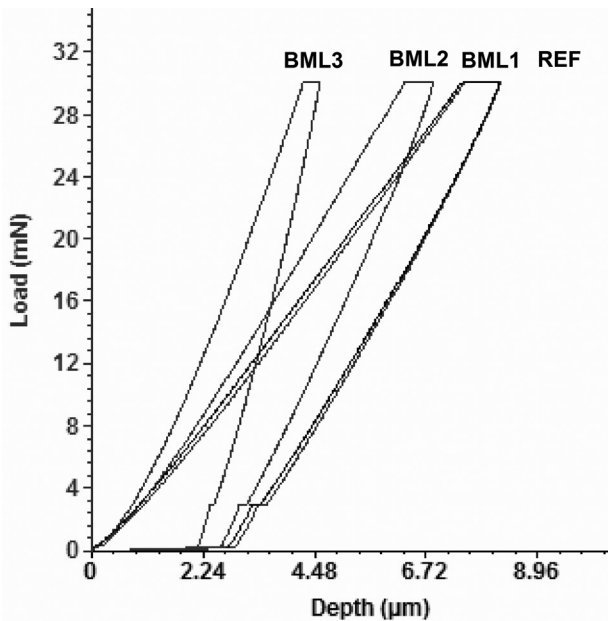


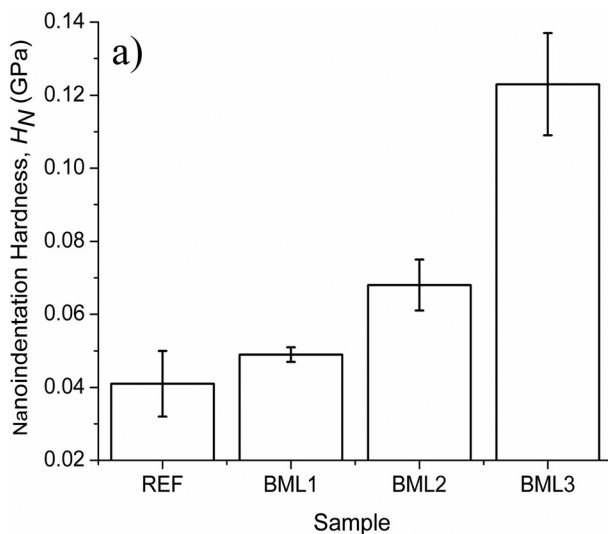
FIG. 5. Load-displacement curves vs. penetration depth at a maximum load of 30 mN for the hot pressed films, as varying the initial number of BML layers.

graphene nanoplatelet particles and causes the changes in the X-ray diffraction.

Figure 4 indicates a clear peak in the (a) panel between the peak labeled G(002)—which is present only in the carbon doped sample—and the second broken line labeled PLA. After hot pressing (Fig. 4(b)), this develops as a broad shoulder both in the carbon doped and in the reference sample, too. This is an indication that the modification that occurred due to hot pressing is linked mostly to the polymer. The G(002) peak is weakly visible even in the hot pressed sample as a small feature on the right side of the first PLA peak.

C. Nanoindentation results

Berkovich nanoindentation is the most common and the most promising contact load testing for determining the



surface mechanical properties of thin films. It has become the reference method for locally measuring the mechanical properties of materials at the nano and microscale. In this study, the hot pressed films were placed on a substrate and subjected to the nanoindentation measurement using Berkovich nanohead at a maximum load of 30 mN. The polycarbonate substrate was chosen in order to minimize the effects of the substrate (much harder or softer than the film) on nanoindentation characteristics. The hardness and the Young's modulus are calculated by Olive-Pharr model (Eqs. (1) and (2)). Fig. 5 presents the load-displacement curves for the hot pressed films as varying the initial number of nanocarbon layers. The curves of the reference PLA film (REF) and the films containing 1 to 3 Black Magic layers (BML1-3) were compared. As seen, the contact indentation depth decreases strongly by increasing the initial number of BML layers, from 7.5 μm for the reference PLA film (REF) and the BML1 film, respectively, to 4.1 μm for the film with 3 nanocarbon layers (BML3). This is associated with increased hardness by increasing the amount of the nanocarbon filler inside the hot pressed film.

Figs. 6(a) and 6(b) present the nanoindentation hardness and Young's modulus of the nanocarbon containing multilayered films with 1 to 3 BML layers as compared to the undoped PLA film used as a reference. Table I summarizes the average values and the standard deviation of the calculated Oliver-Parr model characteristics. The nanoindentation hardness and Young's modulus increase gradually by increasing the number of BML layers in the films, due to increase of the amount of nanocarbon filler. Thus the hot pressed films containing 3 nanocarbon layers (BML3) show about 200% increase of hardness and $\sim 366\%$ increase of elastic modulus if compared to the reference PLA film (REF).

D. Nanoscratch characteristics

The scratch test is currently used as a standard test procedure for surface mechanical properties characterization. It consists in pulling a diamond stylus over the surface of a sample under a normal force. In our case, we apply the nanoscratch

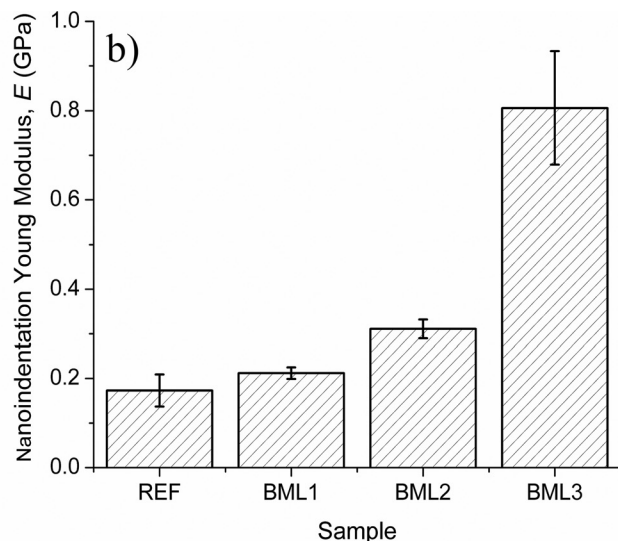


FIG. 6. Comparison of (a) nanoindentation hardness and (b) Young's modulus of the hot pressed multilayered films containing 1–3 BML layers, as well as the reference PLA film (REF).

TABLE I. Summarized mean values and standard deviations for the nanoindentation and nanoscratch characteristics of multilayered thin films as a function of the number of nanocarbon layers.

Sample short name	Berkovich nanoindentation		Nanoscratch with spherical-conical stylus			
	Nanoindentation hardness, H_N (GPa)	Young modulus, E (GPa)	Scratch hardness H_S (GPa)	Scratch coeff. Friction (SCOF)	Normal force F_Z (mN)	Friction force F_f (mN)
REF	0.041 ± 0.009	0.173 ± 0.036	0.417 ± 0.130	1.08 ± 0.190	16.47 ± 9.09	19.443 ± 1.727
BML1	0.049 ± 0.002	0.212 ± 0.013	0.355 ± 0.100	1.111 ± 0.200	14.00 ± 3.90	15.554 ± 0.780
BML2	0.068 ± 0.007	0.311 ± 0.021	0.577 ± 0.217	1.085 ± 0.150	22.77 ± 8.57	24.705 ± 1.286
BML3	0.123 ± 0.014	0.806 ± 0.127	0.684 ± 0.082	1.600 ± 0.250	27.00 ± 3.23	43.200 ± 0.807

loading procedure for characterization of the supported hot pressed films. The scratch hardness and the coefficient of friction are determined at a certain penetration depth. Figs. 7(a) and 7(b) give graphical representations of the calculated values for scratch hardness (H_S) and scratch friction coefficient (SCOF), comparing the reference PLA film and the multilayered films containing 1 to 3 BML layers. Table I summarizes the statistical data (mean values and standard deviations) of nanoscratch characteristics from all conducted experiments.

The results demonstrate that the scratch hardness gradually increase by increasing the number of initial nanocarbon (BML) layers, thus the highest value was obtained for the sample BML3 corresponding to $\sim 64\%$ increase of hardness compared to the reference PLA film (REF). The corresponding maximum normal force at $10 \mu\text{m}$ penetration depth, F_Z , shows a similar tendency. This means that when penetrating the pressed film of 3 BML layers, the tip of the indenter comes across more nanocarbon particles at this penetration depth compared to the films with a smaller number of BML layers. While the scratch coefficient of friction for the thin films has values almost similar to the reference PLA film, insufficiently depending on the number of initial BML layers. The data scattering (i.e., the standard deviations) for the values of both scratch characteristics is relatively high, which can be a sign of the non-homogenous distribution of the nanocarbon particles of the BML layers infiltrated among the polymer layers, leading to the formation of carbon rich and carbon poor regions in the hot pressed films.

E. Microwave and THz properties of hot pressed samples

No frequency dependence of the EM response properties was observed in Ka-band (26–37 GHz), that is why all data

are present for a given frequency, 30 GHz. The thickness of all samples is $10 \mu\text{m}$. One can see from Fig. 8 that the base plastic being $10 \mu\text{m}$ thick is absolutely transparent for microwave radiation, whereas adding only one nanocarbon doped layer of Black Magic filaments decreases the transmittance level to 70% mostly due to the absorption (approx. 25%). The absorption increases continuously as the number of nanocarbon doped layers increases in the sandwich structure (40%). At the same time, the reflection also increases to 20%. Finally, as summarized in Fig. 8, EMI SE (or $-S_{21}$) is as high as 1.5, 2.2, and 4 dB for 1 to 3 nanocarbon doped layers being $10 \mu\text{m}$ thick.

In spite the fact 3D printed initial structures containing three nanocarbon layers are opaque for the microwave radiation, the absorption provided by them ($800 \mu\text{m}$ thick) is less (30%)⁷ in comparison with that observed for hot pressed 3D printed sample being 80 times thinner ($10 \mu\text{m}$), i.e., 40%. Obviously, the difference in the electromagnetic response of initial 3D-printed and hot pressed samples is due to the difference in their thickness as well as their structure: (i) the sandwich structure of original samples with carbon containing layers (10 wt. % of nanocarbon additives), of which EM response is governed mostly by the reflection from the front edge and (ii) hot pressed homogeneous thin films, in which the laminated structure is completely lost and the concentration of the filler becomes less than 10 wt. %.

The absolute values of the complex transmission function (transmittance) in THz range for reference sample and samples contacting 1–3 nanocarbon layers are presented in Fig. 9. In THz frequency range, the transmittance of the base plastic is around 90%–100% and decreases with the frequency. As compared to a microwave range, the frequency dependence of carbon-containing samples is more pronounced and determined by the dispersion of the

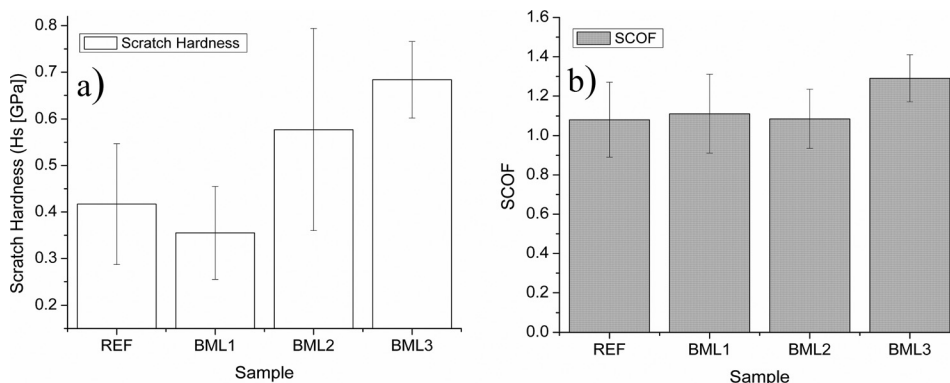


FIG. 7. Mean values and standard deviation of (a) scratch hardness H_S (GPa), and (b) scratch coefficient of friction SCOF of films as varying the initial number of nanocarbon layers.

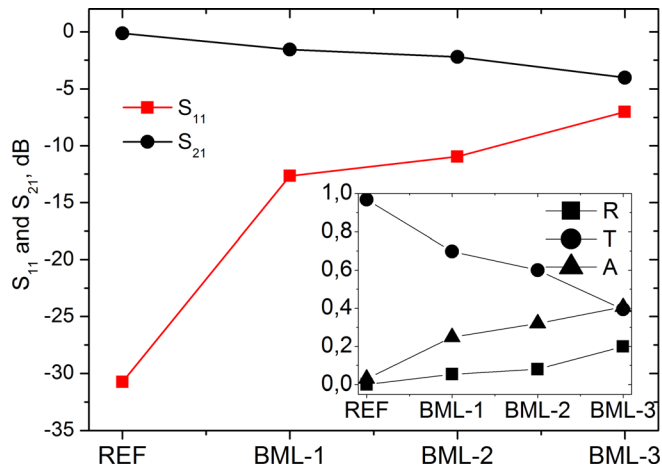


FIG. 8. Measured S-parameters of hot pressed sandwich structures in dB at 30 GHz. Inset: Reflectance, absorbance, and transmittance reconstructed from the experimental data of reference sample and samples contacting 1–3 nanocarbon layers at 30 GHz.

dielectric permittivity of resultant carbon-containing composites produced by hot pressing (see Fig. 10). Addition of only one nanocarbon layer strongly reduces the transmittance level to 60% and 50% for the samples consisting of 1 to 2 and 3 BML at 0.5 THz.

F. Mechanical and electromagnetic properties: Common tendencies

In the case of the hot-pressed 3D-printed samples, each extra layer results in the increase of the nano-carbon concentration. Figure 10 presents the dependence of the real part of the dielectric permittivity, ϵ' conductivity in the THz frequency range, and the mechanical properties vs. the number of layers in the original sample (or filler concentration, wt.%) after hot pressing. The details of dielectric permittivity reconstruction can be found in Ref. 7. The frequency dependence of the real and imaginary part of permittivity for BML2 shows a similar behavior lying between the curves presented in Fig. 10(a), and was omitted in order to not

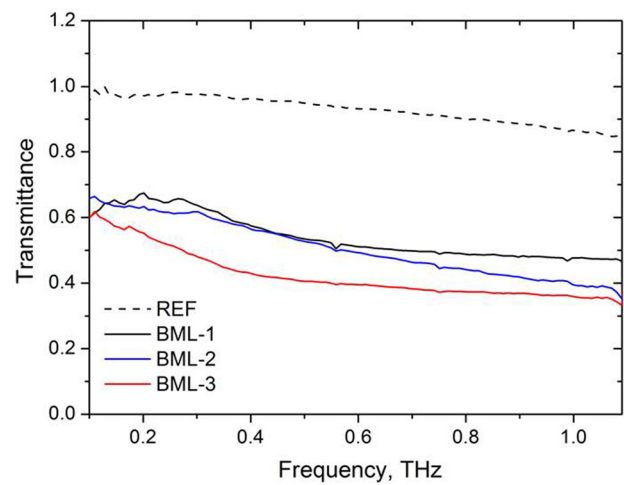


FIG. 9. Terahertz transmittance spectra of the reference sample and samples contacting 1–3 nanocarbon layers.

overload the graph. One can see that $Re(\epsilon)$ and $Im(\epsilon)$ decrease with increasing frequency, while their absolute values are close, especially in high frequency range 200–600 GHz ($\tan \delta \sim 1$). The analogous behavior was observed for polymer composites filled with carbon nanotubes^{19–21} in case of long tubes for which no EM screening effect of inner walls takes place, and the CNT concentration is well above the percolation threshold.²² The physical analysis of the observed dependencies can be done using Maxwell Garnett approximation for an effective medium combined with the Drude-Lorentz model describing the frequency dispersion of the electromagnetic response of the individual inclusions. Thus in the microwave range, the EM response is denoted by the Drude behavior, whereas in THz range, the contribution of Lorentz term is determinative.

Comparative analysis of the mechanical (Young's modulus) and electromagnetic properties (data are presented only for the THz range) is shown in Figure 10(b) vs. the number of BML layers (or nanocarbon concentration in hot pressed sample). An important feature of the composites obtained by

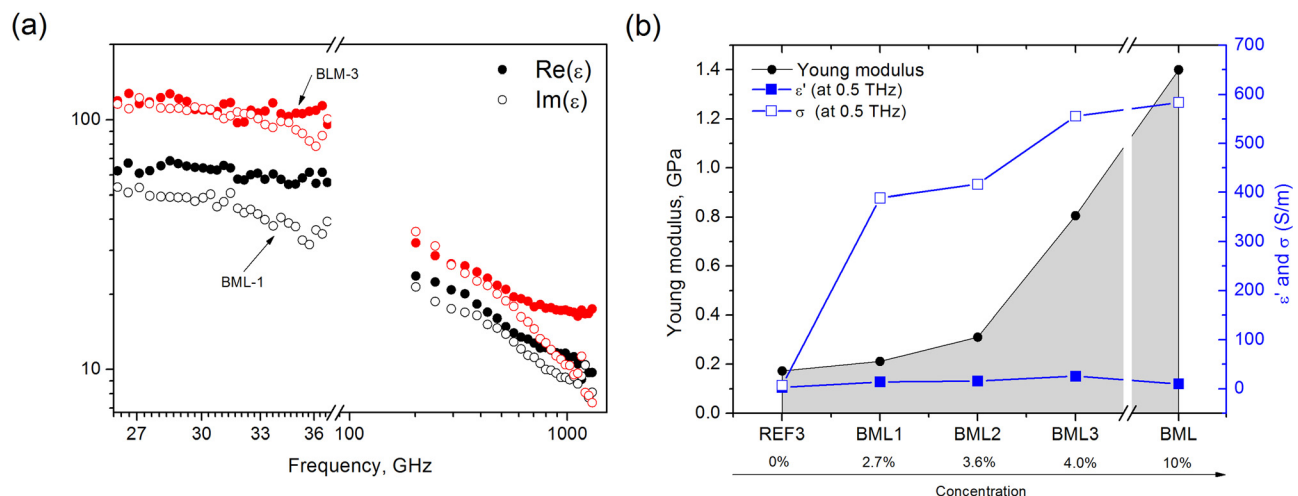


FIG. 10. (a) Frequency dependence of $Re(\epsilon)$ and $Im(\epsilon)$ for BML1 and BML3 samples. (b) The dependence of the real part of the dielectric permittivity and conductivity in the THz frequency range, and the mechanical properties (black curve) on the number of layers in the original sample (or filler concentration, wt.%) after hot pressing.

hot pressing is the possibility to control precisely the concentration of nanocarbon fillers through the varying of the layer thickness in the initial 3D printed structure and the number of layers. It is important that the maximal possible concentration for hot pressed sample could be 6 wt. % for “infinite” number of layers in the initial sandwich structure consisting of the PLA substrate and equal numbers of PLA and BML (10 wt. % of nanocarbon additives) layers.

There are quite a lot of papers devoted to modeling^{23–25} and experimental observation²⁶ of dependencies of physical properties of composites vs. their microstructure. Many factors have to be taken into account such as (i) functional additives filling fraction, (ii) their functional property, (iii) geometrical parameters (including aspect ratio^{27–29}), (iv) percolation threshold and concentration at which saturation of particular physical properties takes place, (v) issues with composite fabrication (i.e., interaction between the filler and matrix³⁰), etc. Sometimes it is possible to observe empirically, the simultaneous variation in filler concentration and physical properties,²³ or even a particular correlation, that is when various characteristics manifest them self differently with the variation of the concentration according to some correlation law.³¹ The case of hot-pressed 3D printed samples is especially interesting because of the tendencies of simultaneous improvement of mechanical, electric, and EM properties of hot-pressed samples shown in Fig. 10(b) for 1...3 BML and pure BML layer (made of black magic filament without adding PLA layers and substrate), could be used for the prediction of physical behaviors of hot pressed samples depending on the number of layers.

IV. CONCLUSIONS

Recently we demonstrated⁷ that 3D printed structures made of BML—commercial composite filament Black Magic¹⁵ based on polylactic acid thermoplastic doped with highly conductive nanocarbon fillers—may have a great potential for electromagnetic compatibility applications in microwave frequency range, giving EMI SE at the level of 8–15 dB being 0.4–1 mm thick. This paper shows that an additional step of samples production such as hot pressing may give extra advantages. In spite of the fact that SAXS and XRD studies showed some amorphization of the nanocarbon filler as a consequence of the hot pressing, resultant material being although 30–10 times thicker than CVD graphene/polymer heterostructure (1–3 μm in total), but still thin enough in comparison with the conventional polymer composites used for applications in the microwave range (1–2 mm),^{32,33} may compete with the CVD graphene sandwiches^{3,5} because of much better processability, and final product cost.

We demonstrate that unlike most conventional composites loaded with nanocarbons, with pronounced dielectric properties ($Re \epsilon \gg Im \epsilon$) at high frequencies, combination of 3D printing and hot pressing allows to fabricate composites with $Re \epsilon \approx Im \epsilon$ in a very broad frequency range (0.2–0.6 THz) and high enough $Re (\epsilon) = 40, 60, 110$ for BML-1, BML-2, BML-3, respectively, at 30 GHz, being at

the same time mechanically robust. That means that much higher absorption ability in comparison with the conventional polymer composites together with much smaller thickness (10–30 μm) could provide high EMI SE.

ACKNOWLEDGMENTS

This work was carried out within the framework of the H2020 Project Nos. 696656 Graphene Core1 and IRSES-2012-318617 FAEMCAR, U.S. Air Force through CRDF Global Agreement Grant No. AF20-15-61804-1, P.K. is thankful for the support by Tomsk State University Competitiveness Improvement Program, A.P. acknowledges FP7 Project No. FP7-316633 POCAONTAS. Authors are thankful to Dr. Konstantin Batrakov, Dr. Alexander Liubimau, and Dr. Mikhail Shuba for fruitful discussions.

¹F. Qin and C. Brosseau, *J. Appl. Phys.* **111**, 061301 (2012).

²P. Kuzhir, A. Paddubskaya, A. Plyushch et al., *J. Appl. Phys.* **114**, 164304 (2013).

³K. Batrakov, P. Kuzhir, A. Paddubskaya et al., *Sci. Rep.* **4**, 7191 (2014).

⁴P. Kuzhir, N. Volynets, S. Maksimenko et al., *J. Nanosci. Nanotechnol.* **13**(8), 5864–5867 (2013).

⁵K. Batrakov, P. Kuzhir, S. Maksimenko et al., *Appl. Phys. Lett.* **108**, 123101 (2016).

⁶R. Kotsilkova, P. Todorov, E. Ivanov et al., *Carbon* **100**, 355–366 (2016).

⁷A. Paddubskaya, N. Valynets, P. Kuzhir et al., *J. Appl. Phys.* **119**, 135102 (2016).

⁸O. Kraft and C. A. Volkert, *Adv. Eng. Mater.* **3**, 99–110 (2001).

⁹R. Zhang, D. Shilo, G. Ravichandran, and K. Bhattacharya, *J. Appl. Mech.* **73**, 730–736 (2006).

¹⁰K. J. Van Vliet and A. Gouldstone, *Surf. Eng.* **17**(2), 140–145 (2001).

¹¹W. C. Oliver and G. M. Pharr, *J. Mater. Res.* **7**, 1564–1583 (1992).

¹²G. M. Pharr, E. G. Herbert, and Y. Gao, *Annu. Rev. Mater. Res.* **40**, 271–292 (2010).

¹³E. Ivanov, I. Borovanska, B. Milosheva, and R. Kotsilkova, “Experimental nano and micro mechanics of nanostructured materials,” in *Mechanics of Nanomaterials and Nanotechnology*, edited by V. Kavardjikov, L. Parashkevova, and A. Baltov, Science Series (Bulgarian Academy of Sciences, 2012), Part IV, Chap. 3, pp. 287–326.

¹⁴R. Saha and W. D. Nix, *Acta Mater.* **50**(1), 23–38 (2002).

¹⁵See <http://www.blackmagic3d.com/Conductive-Graphene-3D-Printing-PLA-Filament-p/grphn-175.htm> for main physical properties, including volume resistivity.

¹⁶K. Geng, F. Yang, T. Druffel, and E. A. Grulke, *Polymer* **48**(3), 841–848 (2007).

¹⁷Z. Wang, A. A. Volinsky, and N. D. Gallant, *J. Appl. Polym. Sci.* **131**(22), 41050 (2014).

¹⁸M. R. VanLandingham, J. S. Villarrubia, W. F. Guthrie, and G. F. Meyers, *Nanoindentation of Polymers: An Overview. Macromolecular Symposia* (NIST, US Department of Commerce, 2001), pp. 15–43.

¹⁹C. Xiang et al., *Ceram. Int.* **33**, 1293 (2007).

²⁰A. Fletcher, M. C. Gupta, K. L. Dudley, and E. Vedeler, *Comput. Sci. Technol.* **70**, 953 (2010).

²¹A. C. Xiang, Y. Pan, X. Liu, X. Sun, X. Shi, and J. Guo, *Appl. Phys. Lett.* **87**, 123103 (2005).

²²M. V. Shuba et al., *Phys. Rev. B* **88**, 045436 (2013).

²³D. K. Hale, *J. Mater. Sci.* **11**, 2105 (1976).

²⁴A. P. Roberts and M. A. Knackstedt, *Phys. Rev. E* **54**, 2313 (1996).

²⁵S. Torquato, *Int. J. Solids Struct.* **37**(1–2), 411–422 (2000).

²⁶L. Vertuccio et al., *Composites Part B* **107**, 192–202 (2016).

²⁷A. Celzard et al., *Phys. Rev. B* **53**(10), 6209 (1996).

²⁸A. Celzard et al., *Carbon* **40**, 2801–2815 (2002).

²⁹A. Celzard and J. F. Mareche, *Physica A* **317**, 305–312 (2003).

³⁰T. Arai et al., *J. Polym. Sci. B: Polym. Phys.* **43**, 2568 (2005).

³¹B. De Vivo et al., *J. Appl. Phys.* **116**, 054307 (2014).

³²D. S. Bychanok et al., *Appl. Phys. Lett.* **103**, 243104 (2013).

³³R. Kotsilkova et al., *Compos. Sci. Technol.* **106**, 85 (2015).